Complexity of segregation behavior at localized deformation sites formed while in service in a 316 stainless steel baffle-former bolt

Timothy G. Lach[1]*, Maxim N. Gussev[2], and Xiang (Frank) Chen[1]
[1]Materials Science and Technology Division, Oak Ridge National Laboratory, Oak Ridge, TN 37831, USA
[2]Nuclear Energy and Fuel Cycle Division, Oak Ridge National Laboratory, Oak Ridge, TN 37831, USA
* Corresponding author: lachtg@ornl.gov

ABSTRACT

Post-irradiation evaluation was performed on a 316 stainless steel baffle former bolt harvested after 40 years of service in a pressurized water reactor. Microstructure analysis revealed the presence of defect-free dislocation channels and strain-induced twins, indicative of loading at a stress level close to yield stress at least once while in service. Primary radiation-induced Ni/Si precipitates were likely destroyed during channel and twin formation, and secondary, significantly coarser Ni/Si precipitates formed inside the newly formed dislocation channels and along ∑3 boundaries during the continued irradiation. Complex chemistry inside the strain-induced features may overlap with dislocation pileups and impact localized corrosion and material long-term performance.

Keywords: in-service radiation; stainless steel; baffle former bolts; radiation-induced segregation (RIS); strain localization

Irradiation-assisted stress corrosion cracking (IASCC) of in-core internal components of pressurized water reactors (PWRs) is one of the critical phenomena that complicates PWR lifespan extension [1–3]. The IASCC primarily results from complex irradiation-induced microstructural and microchemical changes, combined with mechanical stress fields and a corrosive environment. However, the exact contribution of these processes to IASCC remains unclear. Research has highlighted the role of localized deformation and development of dislocation channeling as contributors to IASCC initiation [4,5]; however, many aspects are not completely understood, including roles of deformation mechanics, fine channel structure, microchemistry at the nanoscale, and processes at the defect-free channel – grain boundary (GB) intersections. Thus, highly localized plastic strain within the channels easily exceeds 100% and may be enhanced by strain-induced twin formation [6], causing elevated stresses at GBs [7,8].

However, most IASCC studies have predominantly focused on model alloys [9,10] or in-service irradiated materials evaluated through lab-scale experiments [11–14]; thus, the deformation processes developed outside the radiation environment. Additionally, in-service irradiated components rarely keep sufficient integrity and quality due to removal and handling. These factors limit the experimental evidence and may lead to a lack of critical details. The current study presents, as believed for the first time, a detailed analysis of dislocation channels that occurred in-service while in an irradiation environment with the resulting microstructure continuing to sustain additional irradiation.

As one of the PWR internals, baffle-former bolts (BFBs) are subjected to significant mechanical stress and neutron irradiation during the plant operation. Over the long operation period, harsh in-service conditions lead to potential degradation, complicating the life extension of existing PWRs. The first degraded BFBs were observed in nuclear power plants in 1989 [15]. In support of evaluating the long-term performance of in-core materials, the U.S. Department of Energy Light Water Reactor Sustainability Program pursued the retrieval of aged structural components for the study of the microstructure, mechanical, and corrosion-related properties including IASCC initiation and growth.

Two high fluence BFBs were removed in 2011 from a Westinghouse PWR. According to non-destructive ultrasonic and visual inspection, both BFBs showed no indication of cracking after being withdrawn from service but did require less torque during removal than the installation torque. The BFBs were sectioned

into three parts: bolt head, mid-shank, and thread sections, as described in [16,17]. The present study focuses on the curved region of the BFB designated #4412 where the bolt head meets the bolt shank, as shown in Figure 1a. The bolt head was exposed to about 41 displacements per atom (dpa) over the lifetime of the bolt, while the mid-shank region received about 34 dpa and the thread section of the bolt received about 29 dpa [18]. Thus, the curved region studied here was exposed to approximately 34-41 dpa; although the exact temperature profile of the bolt is unknown, the operating temperature at this portion of the bolt was likely about 305-317 °C [3]. There is also a gradient in gamma radiation and neutron energy along the length of the bolt [19]; however, the focus in the curved region of the bolt can unlikely resolve the effects of the gradient at such a small length scale. As mentioned, there was a reduction in torque required to remove the bolt, so there should be some stress relaxation during operation; however, it is unknown when this happened or whether there were stress fluctuations or other operational stresses. The most important aspect is this section of the bolt still has its in-service exposed surface preserved during handling, which is of high interest because it has higher stress concentration compared to the rest of the bolt head or shank and was also exposed to the primary water [3]. Thus, this region had the primary components for IASCC: corrosive environment, stress, and irradiation.

A slice of the bolt curved region was polished to mirror-finish with colloidal silica polishing as the final step. The cross-section of the near-surface area in the curved region was characterized by scanning electron microscopy (SEM)-electron backscatter diffraction (EBSD) using a Tescan Mira3 SEM equipped with an Oxford Instruments Symmetry S2 EBSD detector. Transmission electron microscopy (TEM) liftouts normal to the surface were made using a Thermo Fisher Versa3D focused ion-beam (FIB)/SEM. The TEM sample preparation followed the procedures of initial trenching, cutting, and thinning to 200 nm with 30 keV Ga^+ beam, thinning to ~100 nm with the ion beam energy gradually reduced to 2 keV. Before loading into the TEM, samples were cleaned with a Fischione 1020 Nanomill for 10 minutes on each side using 900 eV Ar^+. Microstructural characterization was performed with transmission Kikuchi diffraction (tKD) using the Tescan Mira3 SEM, and TEM/ scanning TEM (STEM) with energy-dispersive spectroscopy (EDS)-based mapping using a Thermo Fisher Talos F200X TEM/STEM.

Figure 1b shows the grain structure of the BFB "circle area." It has a dominating annealed austenite structure with equi-axial grains and the presence of abnormal grains (AGs), a result of accelerated growth of some grains, a process often called "abnormal grain growth" [20]. The EBSD kernel average misorientation (KAM) map, Figure 1c, shows low dislocation density in the equi-axial grains. The AG population shows multiple in-grain low-angle boundaries and overall elevated dislocation density, visible as color variations in the inverse pole figure (IPF) map and green region in the KAM map. The AGs have elongated shapes parallel to the BFB surface and often form specific chains, likely reflecting deformation processes during BFB manufacturing.

A thin near-surface layer along the BFB surface is of special interest for the present work. This layer, having a thickness of ~20-25 μm and elevated KAM values, Figure 1c, reflects accumulated plastic deformation due to the BFB processing, handling, installation, and in-service loading events. Analysis of this layer, as believed, may allow for revealing the component history. Thus, scratches may appear in the EBSD maps as artefacts related to specimen preparation. Usually, scratches intersect GBs without changing directions. Scratches do not follow (111) plane slip traces except as a coincidence and are easy to exclude. If artefacts are excluded, the remaining plastic deformation is a combined result of pre-service and in-service deformation processes. Pre-service plastic deformation is also easy to exclude: deformation in non-irradiated austenitic steel occurs along multiple fine slip lines in contrast to coarse dislocation channels in irradiated steel [21,22]. This mechanism generates smooth in-grain lattice orientation gradients, in contrast to sharp, localized "hot spots" in irradiated steel [23].

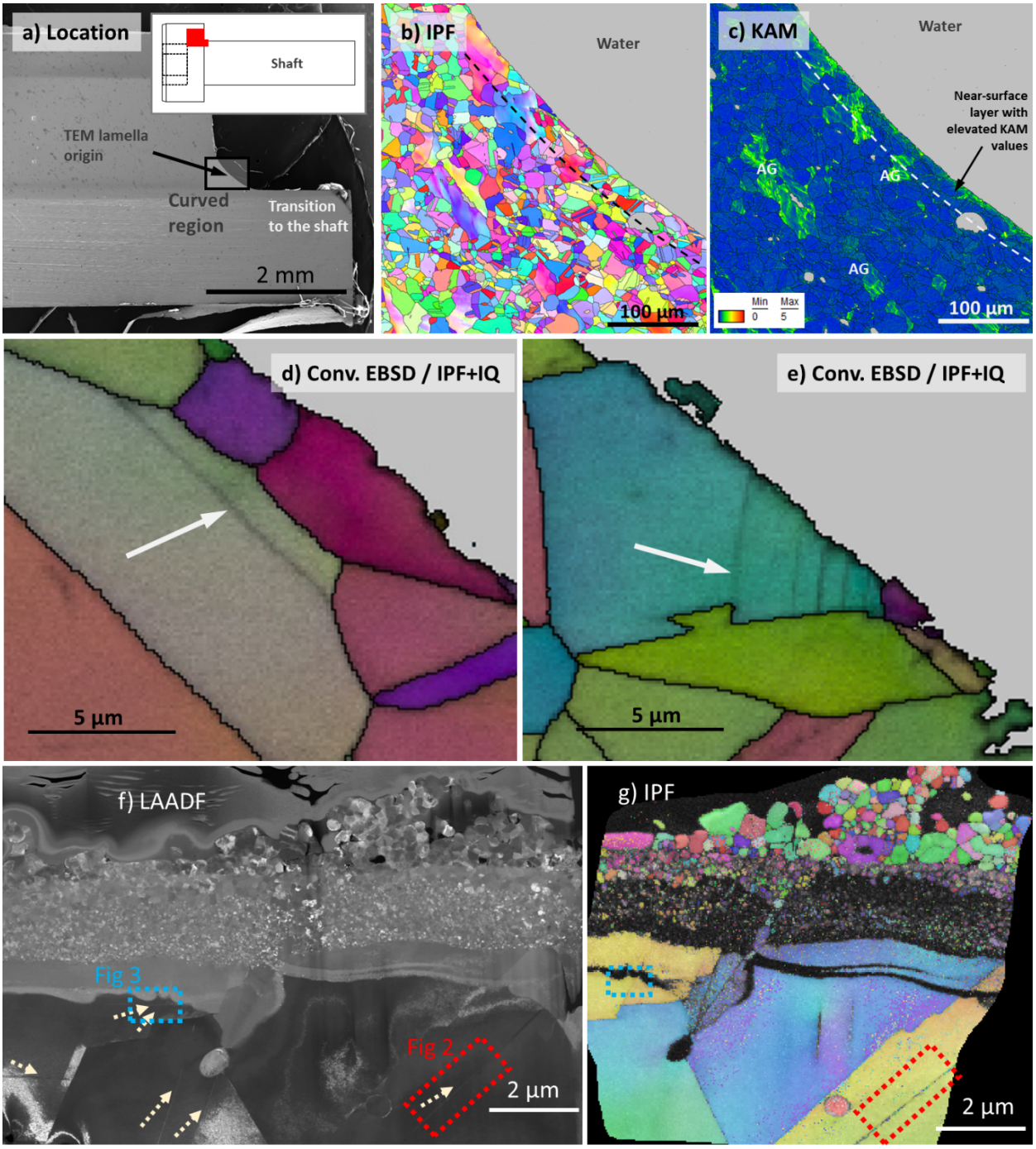

Figure 1. a) Analyzed location of the investigated baffle former bolt (BFB); b,c) EBSD maps representing grain structure at the head-to-shaft transition area. The dashed line in IPF and KAM maps limits the near-surface layer with elevated KAM values. "AG": abnormal grains. Overlapped EBSD IPF and IQ maps showing in-service formed dislocation channels (white arrows). d) Conventional EBSD map showing channel formed in a sub-surface grain; e) EBSD map, demonstrating a series of channels formed in the near-surface grain; f) STEM-LAADF image and g) tKD IPF map of a FIB-liftout taken from the oxidized surface of the curved region. Dotted boxed regions in (f, g) highlight regions analyzed in Figures 2/3. Dotted arrows in (f) point to localized deformation features. The surface and grain boundary oxidation will be the subject of future work.

If pre-irradiation plastic deformation is excluded, some remaining features appear as dark lines starting and ending at GBs, Figure 1d. The typical feature exists within one grain, and its appearance closely resembles

the defect-free channel typically observed in irradiated and deformed austenitic stainless steels [24]. Figure 1e demonstrates a group of similar features that belong to one grain; spacing between these features is ~1-2 μm, a typical distance for dislocation channel spacing [21]. The liftout shown in Figure 1f/g has several strain-induced channel features, as noted by the dotted arrows. Two of these areas are discussed in Figures 2/3. The channels each have different and complex structural features, such as twins and variation in segregation/ precipitation behavior.

Figure 2 shows tKD analysis for the red boxed regions from the liftout in Figure 1f/g with strain-induced features: dislocation channels intersecting the field of view. The channel in the band contrast, IPF, and KAM maps in Figure 2a-c has twin across its length. The KAM values reach up to 2° at the channel boundary, and the cumulative disorientation across the channel is near 60°, which is indicative of a strain-induced twin with two Σ3 boundaries.

STEM-bright field (BF), low angle annular dark field (LAADF), STEM-EDS analysis, and TEM-BF imaging, as shown in Figure 2e-j, were conducted at the same ~50 nm wide feature. The most notable aspect is in the EDS map in Figure 2f showing clear segregation along channel boundaries. The surrounding matrix has a high density of Ni/Si-rich clusters, but there is an excess of clusters along the boundaries. The EDS concentration profile in Figure 2g based on the boxed region in Figure 2f shows the Ni/Si enrichment corresponds with a depletion of Cr, Mo, and Mn; there may be a slight enrichment of P within the channel though it is minimal. Additionally, the Ni and Si concentration between the boundaries is below that of the matrix outside the channel. The lack of precipitates between the boundaries suggests this is a defect-free dislocation channel, the result of localized deformation. There may also be a denuded zone where there is a slight reduction of Ni/Si relative to the matrix just outside the channel. Qualitatively, these results agree with previous studies on radiation-induced segregation (RIS) to GBs, in particular to Σ3 boundaries. [25–27].

The lack of precipitates inside the channel does not mean that no defects are observed within the channel. Nanoscale cavities and dislocation loops are observed within the channel in the under and over-focus TEM-BF images in Figure 2h/i and the TEM-BF image in Figure 2j, respectively. The nanocavities are in high density throughout the matrix just as reported elsewhere [18]. There appear to be fewer cavities within the channel, though it is difficult to quantify if there is a significant difference between the matrix and within the channel boundaries. However, there do appear to be cavities that build up on the channel boundaries as denoted by the dotted arrows. Similarly, the dislocation loop density appears to be much lower within the channel than in the matrix, as noted in Figure 2j. Taken together, the total density of defects including precipitates, nanocavities, and dislocation loops are lower within the channel.

Although segregation at Σ3 boundaries, particularly coherent Σ3 boundaries, is weaker compared to random high-angle grain boundaries (RHAGBs) [26], this process cannot be dismissed. While there is evidence of twinning in the channel in Figure 2, destruction of Ni/Si-rich precipitates suggests the passage of multiple dislocations along the channel, since a single twinning event would likely be insufficient to destroy precipitates [28]. The motion of dislocations, especially through heavy or severe deformation, has been shown to dissolve precipitates [29,30] and is likely what happens here at the local scale.

It is important to emphasize that the reprecipitation on the channel boundaries suggests continued RIS and precipitation after its formation. The exact deformation mechanics may be complicated [31] but are outside the present work scope.

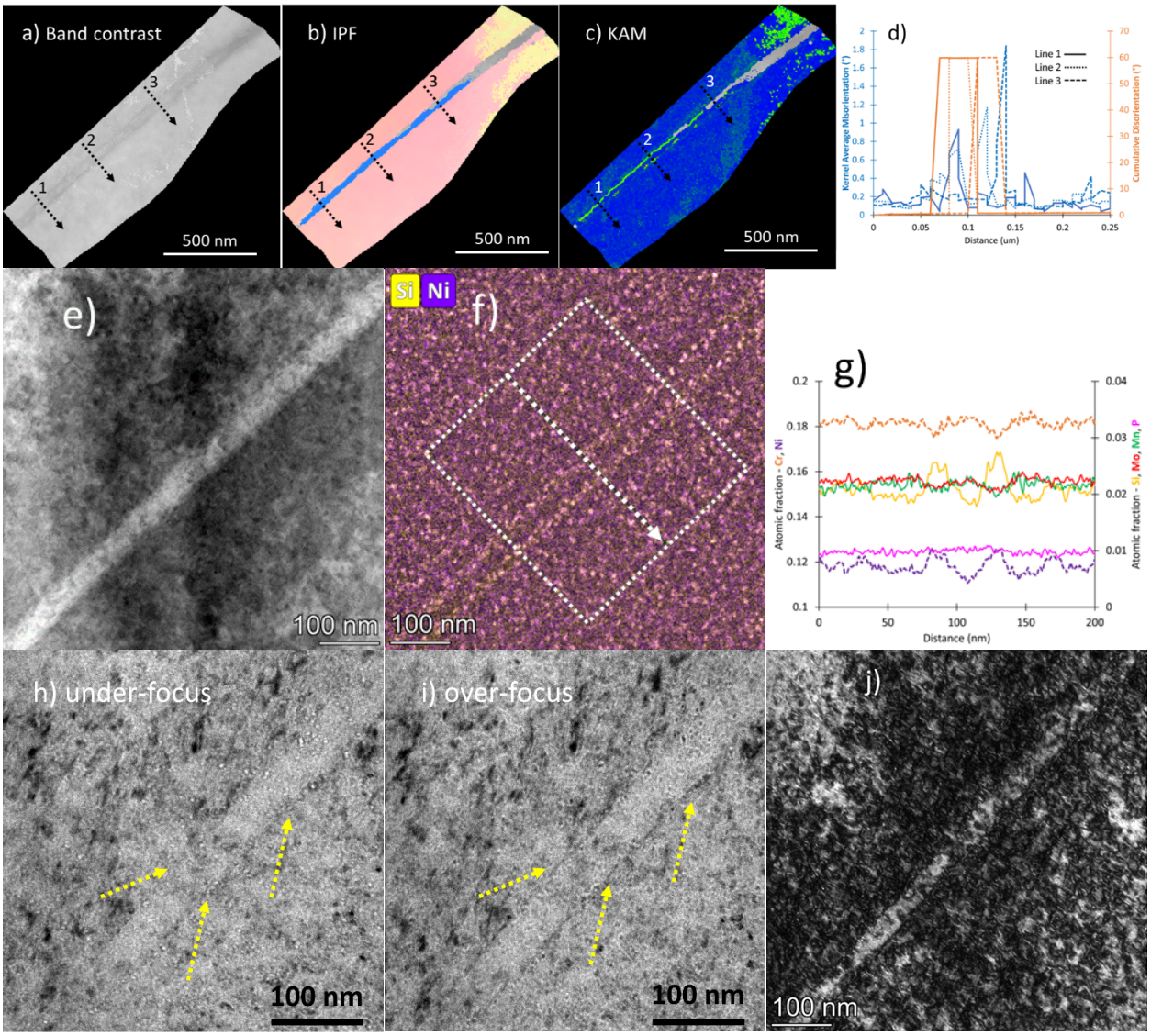

Figure 2. tKD a) band contrast, b) IPF, and c) KAM maps with 5 nm step size of red dotted box in Figure 1 showing strain induced channel with deformation twin occupying most of the channel; d) KAM and cumulative disorientation point-to-point profiles #1–#3 shown in a-c); e) STEM-BF and f) STEM-EDS Ni and Si map of same channel; g) concentration profile based on box in f) across the channel; h) under-focus and i) over-focus TEM-BF images highlighting nanocavities including those along channel boundaries (arrows); and j) TEM two-beam BF image showing dislocation loops in matrix and channel.

Similar STEM-EDS analyses were completed on other channel and localized defect features as well. The blue-boxed region in Figure 1f/g is characterized with STEM imaging and STEM-EDS analysis in Figure 3. This region shows two localized dislocation channels, DC_1 and DC_2, Figure 3a – the near vertical one (DC_1) and the horizontal one (DC_2). The DC_1 channel has extensive Ni/Si segregation and Cr/Mo/Mn depletion at the channel boundaries, Figure 3d, more so than the channel boundaries in Figure 2. Two maximums in Si and Ni curves suggest strain-induced twins occupying a portion of the DC_1 channel. However, instead of discrete precipitates, the segregation to the channel boundaries appears to be smooth here and reaches a much higher level than the channel in Figure 2. The BF and LAADF images show there is some but relatively low dislocation content within the channel. The DC_2 channel on the other hand has elongated diffraction features as dislocations passed along it. This channel intersects with the other channel and looks like it causes DC_1 channel to bend or be compressed slightly (the bending is pointed by dashed arrow in Figure 3a,b). This horizontal channel does have some slight Ni/Si segregation to it, Figure 3c but

no evidence of a strain-induced twin. The higher degree of segregation at the DC_1 channel boundaries in Figure 3 also means these boundaries may likely be incoherent Σ3 boundaries due to being a good sink for defects and solute and comparable to RHAGBs [26]. The segregation to the non-twinned channel suggests that localized strain-induced features can serve as sinks for defects and solutes just as a dislocations and dislocation cells can [32].

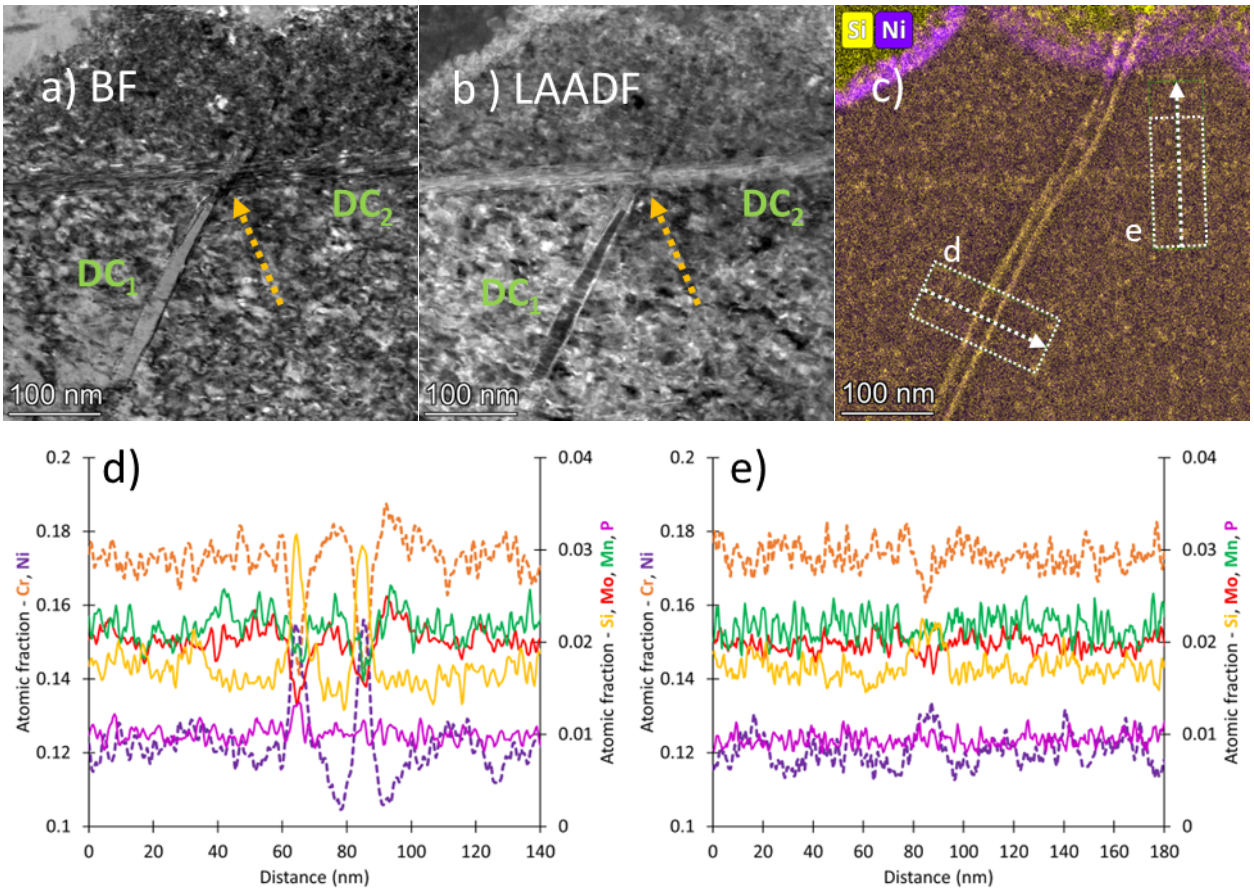

Figure 3. a) STEM-BF, b) STEM-LAADF, and c) STEM-EDS Ni and Si map of blue dotted box in Figure 1 showing dislocation channel (DC_1) with likely internal twin intersecting with another dislocation channel (DC_2); d) concentration profile based on box in c) across the channel DC_1; e) concentration profile based on box in c) across the channel DC_2.

Generalizing, the results confirm the presence of localized deformation features (defect-free channels with or without twins) formed in the component during its in-service life. The discussed features suggest that the BFB was mechanically loaded, and the material reached levels of stress that were close to or even exceeded the yield stress (YS). Defect-free channels may form at stress levels as low as ~0.8 YS in a routine tensile test, with a strain rate of ~10^{-3} s^{-1} [33] and at ~0.5 YS during slow strain rate testing (~10^{-7} s^{-1}) [34]. Although the exact stress level, loading rate, and time of loading event(s) are under question, multiple strain-induced defects, typical for irradiated steel, undoubtedly indicate episodical loading during service.

The timeline is an interesting and practically important question. Channel formation requires damage doses of only ~1 dpa [35]. Thus, the observed strain-induced features formed after some damage dose and likely at different times during operation. However, secondary RIS and precipitation at the channels and along the channel walls and the presence of a limited density of nanocavities and dislocation loops, particularly inside twinned channels, suggest these channels formed no more than about 1-5 years (or 1-5 dpa) before BFB extraction from the reactor. Such a time (dose) is needed to recreate the Ni/Si-segregation structure and secondary RIS at newly formed Σ3 boundaries. Likely, this time could not be too long (tens dpa), or the channel would be filled with new radiation defects. The density of nanocavities and particularly loops

was much lower than the surrounding matrix. Although "pure" dislocation channeling is usually expected for straining at the reactor operating temperatures of ~280-340 °C [5,7], deformation twins were observed as well [6]. Thus, twin presence cannot serve as evidence of room-temperature deformation.

Secondary RIS strongly suggests that the defect-free channel contribution to different phenomena (e.g., dislocation channeling as a driving force for IASCC [1]) may extend beyond purely mechanical effect and contribution of dislocation pileups [22], observed in model experiments with pre-irradiated materials. Dislocation channels may serve as traps for defects as evidenced by the precipitates that formed along them. However, they could also serve to enhance solute diffusion [36,37] as the degree of strain locally can reach greater than 100% [38]. A synergistic effect could also take place as dislocations create a higher concentration of solute locally [28], which could mediate solute diffusion towards the grain boundary while also creating solute trapping sites with the matrix enabling precipitation along the channel walls. This change in solute concentration locally may affect not only the mechanical stress and strain locally but also the response to corrosive environments. Enhanced Ni/Si segregation in the in-service formed channels may lead to variations in local corrosion behavior on a subgrain scale, which could further enhance susceptibility to IASCC. The observed behavior here needs additional, focused investigation through controlled experiments with the exact stress level and loading event timing. Such experiments could involve materials under mechanical load during irradiation [39] or combined radiation and corrosion [40,41] to understand the effects of extended radiation and corrosion on previously formed dislocation channels.

Declaration of Competing Interest

The authors declare that they have no known competing financial interests or personal relationships that could have appeared to influence the work reported in this paper.

Acknowledgments

The research was supported by the US Department of Energy, Office of Nuclear Energy, Light Water Reactor Sustainability Program Materials Research Pathway. This manuscript has been authored by UT-Battelle, LLC, under contract DE-AC05-00OR22725 with the US Department of Energy (DOE). The US government retains and the publisher, by accepting the article for publication, acknowledges that the US government retains a nonexclusive, paid-up, irrevocable, worldwide license to publish or reproduce the published form of this manuscript, or allow others to do so, for US government purposes. DOE will provide public access to these results of federally sponsored research in accordance with the DOE Public Access Plan (http://energy.gov/downloads/doe-public-access-plan). The authors would like to thank Patricia Tedder and Travis Dixon at the Low Activation Materials Development and Analysis (LAMDA) Laboratory at ORNL, where SEM and TEM/STEM evaluation was conducted. Microscopy in LAMDA is a cost recovery center available for users through the US-DOE Nuclear Science User Facilities. The Thermo Fisher Talos 200X STEM in LAMDA was purchased and funded through the US-DOE Office of Nuclear Energy Advanced Fuel Campaign and Nuclear Science User Facilities. The authors would like to thank the late Mike Burke who was involved in the bolt harvesting and characterization planning and led the sample preparation, machining, and shipping when he was working at Westinghouse Electric Company.

References

[1] G.S. Was, C.-B. Bahn, J. Busby, B. Cui, D. Farkas, M. Gussev, M. Rigen He, J. Hesterberg, Z. Jiao, D. Johnson, W. Kuang, M. McMurtrey, I. Robertson, A. Sinjlawi, M. Song, K. Stephenson, K. Sun, S. Swaminathan, M. Wang, E. West, How irradiation promotes intergranular stress corrosion crack initiation, Prog. Mater. Sci. 143 (2024) 101255. https://doi.org/10.1016/j.pmatsci.2024.101255.

[2] T. Shoji, S. Suzuki, K.S. Raja, Current status and future of IASCC research, J. Nucl. Mater. 258–263 (1998) 241–251. https://doi.org/10.1016/S0022-3115(98)00304-3.

[3] M.R. Ickes, J. McKinley, J.-K. Lee, J.M. Smith, A.M. Ruminski, M.A. Burke, Irradiation-assisted stress corrosion cracking of Type 347 and Type 316 steels irradiated in commercial pressurized water reactors, J. Nucl. Mater. 536 (2020) 152182. https://doi.org/10.1016/j.jnucmat.2020.152182.

[4] B. Margolin, A. Sorokin, N. Pirogova, A. Toivonen, F. Sefta, C. Pokor, Analysis of mechanisms

inducing corrosion cracking of irradiated austenitic steels and development of a model for prediction of crack initiation, Eng. Fail. Anal. 107 (2020) 104235. https://doi.org/10.1016/j.engfailanal.2019.104235.
[5] Z. Jiao, G.S. Was, Impact of localized deformation on IASCC in austenitic stainless steels, J. Nucl. Mater. 408 (2011) 246–256. https://doi.org/10.1016/j.jnucmat.2010.10.087.
[6] T. Onchi, K. Dohi, N. Soneda, J.R. Cowan, R.J. Scowen, M.L. Castaño, Fractographic and microstructural characterization of irradiated 304 stainless steel intergranularly fractured in inert gas, J. Nucl. Mater. 320 (2003) 194–208. https://doi.org/10.1016/S0022-3115(03)00105-3.
[7] K.J. Stephenson, G.S. Was, The role of dislocation channeling in IASCC initiation of neutron irradiated stainless steel, J. Nucl. Mater. 481 (2016) 214–225. https://doi.org/10.1016/j.jnucmat.2016.09.001.
[8] P.L. Andresen, G.S. Was, A historical perspective on understanding IASCC, J. Nucl. Mater. 517 (2019) 380–392. https://doi.org/10.1016/j.jnucmat.2019.01.057.
[9] J.T. Busby, G.S. Was, E.A. Kenik, Isolating the effect of radiation-induced segregation in irradiation-assisted stress corrosion cracking of austenitic stainless steels, J. Nucl. Mater. 302 (2002) 20–40. https://doi.org/10.1016/S0022-3115(02)00719-5.
[10] D. Du, K. Sun, G.S. Was, IASCC of neutron irradiated 316 stainless steel to 125 dpa, Mater. Charact. 173 (2021) 110897. https://doi.org/10.1016/j.matchar.2021.110897.
[11] A.G. Penders, M.J. Konstantinović, W. Van Renterghem, R.-W. Bosch, D. Schryvers, F. Somville, Characterization of IASCC crack tips extracted from neutron-irradiated flux thimble tube specimens in view of a probabilistic fracture model, J. Nucl. Mater. 571 (2022) 154015. https://doi.org/10.1016/j.jnucmat.2022.154015.
[12] R.-W. Bosch, W. Van Renterghem, S. Van Dyck, R. Chaouadi, R. Gérard, F. Somville, Microstructure, mechanical properties and IASCC susceptibility of stainless steel baffle bolts after 30 years of operation in a PWR, J. Nucl. Mater. 543 (2021) 152615. https://doi.org/10.1016/j.jnucmat.2020.152615.
[13] O.K. Chopra, A.S. Rao, A review of irradiation effects on LWR core internal materials – IASCC susceptibility and crack growth rates of austenitic stainless steels, J. Nucl. Mater. 409 (2011) 235–256. https://doi.org/10.1016/j.jnucmat.2010.12.001.
[14] K.J. Stephenson, G.S. Was, Comparison of the microstructure, deformation and crack initiation behavior of austenitic stainless steel irradiated in-reactor or with protons, J. Nucl. Mater. 456 (2015) 85–98. https://doi.org/10.1016/j.jnucmat.2014.08.021.
[15] P. Scott, A review of irradiation assisted stress corrosion cracking, J. Nucl. Mater. 211 (1994) 101–122. https://doi.org/10.1016/0022-3115(94)90360-3.
[16] X. (Frank) Chen, K.J. Leonard, M.A. Sokolov, M.A. Burke, M.N. Gussev, S.R. Clark, Specimen Fabrication from Two High Fluence Ginna Baffle Bolts, ORNL/TM-2017/455, 2017.
[17] T.G. Lach, X. (Frank) Chen, T.M. Rosseel, Microstructural characterization of the second high fluence baffle-former bolt retrieved from a Westinghouse two-loop downflow type PWR, ORNL/TM-2022/2668, 2022. https://doi.org/10.2172/1897832.
[18] T.G. Lach, X. (Frank) Chen, Post Irradiation Examination of Pressurized Water Reactor Stainless Steel Internal Components, in: Press. Vessel. Pip., 2023: p. 107347. https://doi.org/10.1115/PVP2023-107347.
[19] D.J. Edwards, E.P. Simonen, F.A. Garner, L.R. Greenwood, B.M. Oliver, S.M. Bruemmer, Influence of irradiation temperature and dose gradients on the microstructural evolution in neutron-irradiated 316SS, J. Nucl. Mater. 317 (2003) 32–45. https://doi.org/10.1016/S0022-3115(03)00003-5.
[20] J. Mizera, J.W. Wyrzykowski, K.J. Kurzydłowski, Description of the kinetics of normal and abnormal grain growth in austenitic stainless steel, Mater. Sci. Eng. A. 104 (1988) 157–162. https://doi.org/10.1016/0025-5416(88)90417-X.
[21] Z. Jiao, J.T. Busby, G.S. Was, Deformation microstructure of proton-irradiated stainless steels, J. Nucl. Mater. 361 (2007) 218–227. https://doi.org/10.1016/j.jnucmat.2006.12.012.
[22] G.S. Was, D. Farkas, I.M. Robertson, Micromechanics of dislocation channeling in intergranular

stress corrosion crack nucleation, Curr. Opin. Solid State Mater. Sci. 16 (2012) 134–142. https://doi.org/10.1016/j.cossms.2012.03.003.
[23] K.G. Field, M.N. Gussev, J.T. Busby, Microstructural characterization of deformation localization at small strains in a neutron-irradiated 304 stainless steel, J. Nucl. Mater. 452 (2014) 500–508. https://doi.org/10.1016/j.jnucmat.2014.05.053.
[24] M.N. Gussev, K.J. Leonard, In situ SEM-EBSD analysis of plastic deformation mechanisms in neutron-irradiated austenitic steel, J. Nucl. Mater. 517 (2019) 45–56. https://doi.org/10.1016/j.jnucmat.2019.01.034.
[25] N. Sakaguchi, S. Watanabe, H. Takahashi, R.G. Faulkner, A multi-scale approach to radiation-induced segregation at various grain boundaries, J. Nucl. Mater. 329–333 (2004) 1166–1169. https://doi.org/10.1016/j.jnucmat.2004.04.268.
[26] C.M. Barr, G.A. Vetterick, K.A. Unocic, K. Hattar, X.-M. Bai, M.L. Taheri, Anisotropic radiation-induced segregation in 316L austenitic stainless steel with grain boundary character, Acta Mater. 67 (2014) 145–155. https://doi.org/10.1016/j.actamat.2013.11.060.
[27] S. Watanabe, Y. Takamatsu, N. Sakaguchi, H. Takahashi, Sink effect of grain boundary on radiation-induced segregation in austenitic stainless steel, J. Nucl. Mater. 283–287 (2000) 152–156. https://doi.org/10.1016/S0022-3115(00)00204-X.
[28] Z. Jiao, M.D. McMurtrey, G.S. Was, Strain-induced precipitate dissolution in an irradiated austenitic alloy, Scr. Mater. 65 (2011) 159–162. https://doi.org/10.1016/j.scriptamat.2011.04.003.
[29] Y. Ashkenazy, N.Q. Vo, D. Schwen, R.S. Averback, P. Bellon, Shear induced chemical mixing in heterogeneous systems, Acta Mater. 60 (2012) 984–993. https://doi.org/10.1016/j.actamat.2011.11.014.
[30] S.N. Arshad, T.G. Lach, M. Pouryazdan, H. Hahn, P. Bellon, S.J. Dillon, R.S. Averback, Dependence of shear-induced mixing on length scale, Scr. Mater. 68 (2013). https://doi.org/10.1016/j.scriptamat.2012.10.027.
[31] M. Griffiths, Strain Localisation and Fracture of Nuclear Reactor Core Materials, J. Nucl. Eng. 4 (2023) 338–374. https://doi.org/10.3390/jne4020026.
[32] J. Yang, L. Hawkins, Z. Shang, E.A. McDermott, B.K. Tsai, L. He, Y. Lu, M. Song, H. Wang, X. Lou, Dislocation channel broadening–A new mechanism to improve irradiation-assisted stress corrosion cracking resistance of additively manufactured 316 L stainless steel, Acta Mater. 266 (2024) 119650. https://doi.org/10.1016/j.actamat.2024.119650.
[33] M.N. Gussev, K.G. Field, J.T. Busby, Deformation localization and dislocation channel dynamics in neutron-irradiated austenitic stainless steels, J. Nucl. Mater. 460 (2015) 139–152. https://doi.org/10.1016/j.jnucmat.2015.02.008.
[34] K.J. Stephenson, G.S. Was, Crack initiation behavior of neutron irradiated model and commercial stainless steels in high temperature water, J. Nucl. Mater. 444 (2014) 331–341. https://doi.org/10.1016/j.jnucmat.2013.10.008.
[35] K. Farrell, T.S. Byun, N. Hashimoto, Deformation mode maps for tensile deformation of neutron-irradiated structural alloys, J. Nucl. Mater. 335 (2004) 471–486. https://doi.org/10.1016/j.jnucmat.2004.08.006.
[36] S. Odunuga, Y. Li, P. Krasnochtchekov, P. Bellon, R.S. Averback, Forced Chemical Mixing in Alloys Driven by Plastic Deformation, Phys. Rev. Lett. 95 (2005) 45901. https://doi.org/10.1103/PhysRevLett.95.045901.
[37] M. Wang, R.S. Averback, P. Bellon, S. Dillon, Chemical mixing and self-organization of Nb precipitates in Cu during severe plastic deformation, Acta Mater. 62 (2014) 276–285. https://doi.org/10.1016/j.actamat.2013.10.009.
[38] M.D. McMurtrey, G.S. Was, B. Cui, I. Robertson, L. Smith, D. Farkas, Strain localization at dislocation channel–grain boundary intersections in irradiated stainless steel, Int. J. Plast. 56 (2014) 219–231. https://doi.org/10.1016/j.ijplas.2014.01.001.
[39] S.A. Briggs, M. Steckbeck, N.M. Heckman, T.A. Furnish, D.C. Bufford, D. Buller, B.L. Boyce, K. Hattar, A combined thermomechanical and radiation testing platform for a 6 MV tandem accelerator, Nucl. Instruments Methods Phys. Res. Sect. B Beam Interact. with Mater. Atoms. 509

(2021) 39–47. https://doi.org/10.1016/j.nimb.2021.08.011.
[40] S.S. Raiman, G.S. Was, Accelerated corrosion and oxide dissolution in 316L stainless steel irradiated in situ in high temperature water, J. Nucl. Mater. 493 (2017) 207–218. https://doi.org/10.1016/j.jnucmat.2017.05.043.
[41] W. Zhou, K.B. Woller, G. (Tony) Zheng, P.W. Stahle, M.P. Short, A simultaneous corrosion/irradiation facility for testing molten salt-facing materials, Nucl. Instruments Methods Phys. Res. Sect. B Beam Interact. with Mater. Atoms. 440 (2019) 54–59. https://doi.org/10.1016/j.nimb.2018.11.024.